Eur. Phys. J. E **26**, 183–189 (2008)
DOI 10.1140/epje/i2007-10303-4

THE EUROPEAN PHYSICAL JOURNAL E

Macroscopic alignment of nanoparticle arrays in soft crystals of cubic and cylindrical polymer micelles

D.C. Pozzo[a] and L.M. Walker[b]

Department of Chemical Engineering (Center for Complex Fluids Engineering), Carnegie Mellon University, Pittsburgh, PA 15213, USA

Received 30 October 2007
Published online: 16 April 2008 –

Abstract. We describe a method to organize nanometer-sized hydrophilic particles into ordered arrays by templating them in the soft, micelle-crystal phases (spherical and cylindrical) of a thermoreversible block copolymer. Small-angle neutron scattering (SANS) with contrast variation is used to show that the dispersed particles (in this case, proteins or silica) form structured arrays by being constrained in the interstitial cavities between the polymer micelles in the ordered micelle crystal. Simple shear is used to macroscopically align both phases of the nanocomposites (micelles and particles) into macro-domains. The temperature-induced order-order transition between templates of spherical and cylindrical micelles is demonstrated as a reversible technique to modify the structure of the templated nanoparticle arrays.

PACS. 81.16.Dn Self-assembly – 61.46.-w Structure of nanoscale materials – 62.23.St Complex nanostructures, including patterned or assembled structures

1 Introduction

A simple method is used to form arrays of nanoparticles that are templated by soft crystals of polymer micelles. Both inorganic (silica) and organic (protein) nanoparticles are amenable to this approach. The micelle template is composed of a tri-block copolymer (Pluronic P123) that is dissolved in water. This report is part of our recent work describing the formation of nanoparticle arrays by templating in the crystalline phases of thermoreversible block copolymers [1–5]. In these soft nanocomposites, the polymer matrix provides mechanical support to the dispersed particles and allows the interparticle separation to be controlled by modifying the structure of the template. Therefore, it allows for the possibility to tailor the macroscopic properties of a material by changing the polymer template.

The tri-block copolymer used in this work consists of a poly-propylene oxide (PPO) center block and two identical poly-ethylene oxide (PEO) end blocks. These polymers have a high solubility in water at low temperatures ($< 5\,^{\circ}$C). Therefore, it is possible to make concentrated solutions with relatively low viscosities while the polymers are in a coil-like conformation. As the temperature is increased, the middle PPO block becomes increasingly hydrophobic. This drives the formation of micelles that can be spherical or cylindrical and that have a dehydrated PPO core and a hydrated PEO corona [6,7]. At high polymer concentrations ($> 15\,$wt% for P123), crystalline phases of these micelles are observed. The structures of these micelle crystals are well characterized for many Pluronic copolymers [6–9]. The micelle crystal phases presented here are solid-like materials with a relatively high elastic modulus ($> 20\,$kPa).

The specific tri-block copolymer used in this work (Pluronic P123) forms spherical or cylindrical micelles depending on the temperature and the polymer concentration. In a narrow concentration range (30–40 wt%), this polymer undergoes a transition from a soft crystal of spherical micelles (cubic packing) into a crystal of cylindrical micelles (hexagonal packing) as the temperature is raised [7]. In this work, we make use of these thermoreversible self-assembling properties to disperse hydrophilic particles in the concentrated polymer solution at low temperatures ($T < 15\,^{\circ}$C) when the viscosity is low. We then increase the temperature to induce the desired micelle crystal phase (spherical or cylindrical micelles). Figure 1 shows a schematic representation of the templated nanocomposites in the spherical and in the cylindrical crystal phases. As the micelle crystals form, the dispersed particles are constrained to the remaining interstitial spaces between the micelles. Therefore, the organization occurs through an organized exclusion of volume as the micelles take most of the sample space. This approach has been shown to work for cubic packing of spherical micelles, here we demonstrate the use of an anisotropic

[a] *Current address:* Department of Chemical Engineering, University of Washington, Seattle WA 98195, USA.
[b] e-mail: lwalker@andrew.cmu.edu

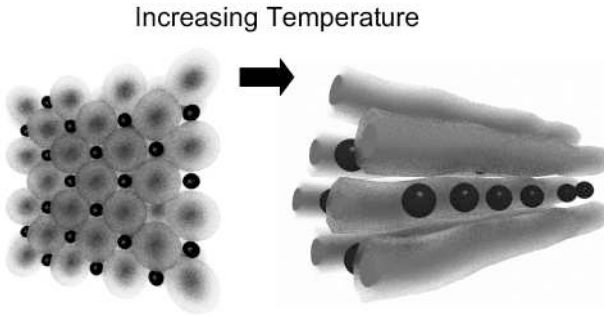

Fig. 1. Schematic representation of the particles (black spheres) templated in the spherical and cylindrical micelle crystal phases of the block copolymer.

packing of cylindrical micelles and the ability to switch between these two structures.

Three different particle additives are used to assess the nanometer scale organization, two different proteins and a synthetic silica nanoparticulate system. The two globular proteins are chosen for their different sizes, lysozyme ($R_H = 1.95\,nm$) [10] and bovine serum albumin ($R_H = 3.39\,nm$) [11], are used as model nanoparticles due to their monodispersity and because their repulsive interaction with the polymer is well characterized [11]. The lack of any specific attraction between these proteins and the polymer chains results in the partitioning of the proteins in the interstitial spaces that are not occupied by the micelles. Placing the native proteins in the solid PPO core of the micelles is largely unfavorable due to the hydrophilic nature of the protein surface. The silica particles are commercially available (Ludox SM) with a nominal diameter of 7 nm and are used to demonstrate the versatility of this templating method in the organization of nanoparticles. Silica has a weakly attractive interaction with PEO but it does not interact with PPO [12]. Therefore, these particles are also located in the interstitial cavities around the micelles. The small size of the PEO blocks of this polymer and the high curvature of the particles hinder strong adsorption on the silica surface [13].

Small-angle neutron scattering (SANS) at contrast-matched conditions is used to independently probe the structure of the micelle template and the particle arrays [14]. This scattering technique allows us to independently probe the internal structure of the two material phases of the same nanocomposite (polymer and particles). In this technique, a mixture of isotopes is used in the solvent (D_2O/H_2O) in order to "match" the scattering length density (SLD) of each of the dispersed materials on two separate experiments. At contrast-matched conditions, the scattering experiments probe the internal structure of the material that is not "matched" by the solvent. The use of solvents with isotope mixtures allows us to change the scattering contrast without drastically altering the chemistry of the solvent [14]. The contrast matching isotope compositions are determined experimentally. For the P123 polymer, this corresponds to a mixture of 13% D_2O and 87% H_2O by mole. The matching point for the proteins is 40% D_2O, 60% H_2O and for the silica it is 61% D_2O, 39% H_2O. The SANS experiments are carried out under shear ($\dot{\gamma} = 10\,s^{-1}$) using a Couette shear cell that is designed for SANS experiments [15]. In our experiments, the incident beam is parallel to the shear gradient.

Templating of nanostructures using cylindrical micelles has been reported in the literature. Bouchama *et al.* use the hexagonal phase of cylindrical surfactant micelles to template metallic nanoparticles in the hydrophobic cores [16]. Alberius and coworkers use the cylindrical micelle structure of Pluronic P123 to direct the synthesis of mesoporous silica and titania [17]. Castelletto, Ansari and Hamley add disc-like clay particles to Pluronic P123 and find that this triggers a transition from arrays of cylindrical micelles to a lamellar phase [8]. Despite these important contributions to this field, it is still necessary to develop simple and versatile methods to organize nanoparticles so that they may be used in a variety of applications. For example, the organization of particles into organized arrays often results in unique optical properties that arise from proximity effects between neighboring particles [18]. It is also demonstrated that plasmon resonance between neighboring noble-metal nanoparticles can be used to efficiently transport light at nanometer length scales [19]. Cylindrical micelle templates, like those discussed here, could be used to generate these linear particle waveguides at macroscopic lengthscales and in a cost effective manner.

In this work, we demonstrate that it is possible to organize nanoparticles, either inorganic or organic, using ordered phases of cylindrical micelles. The use of a thermoreversible polymer allows us to disperse existing nanoparticles without requiring particle synthesis inside the polymer matrix [1–5]. Therefore, this method can be used to organize a wide variety of nanosized particulate materials including biological components like globular proteins. We also demonstrate that shear can be used to align the micelle template into a crystal where most of the cylinders have the same general orientation (macroscopic domain). This shear alignment of the micelle template also results in the macroscopic orientation of the linear particle arrays. Finally, we demonstrate that temperature can be used to trigger an order-order transition from crystals of spherical micelles into crystals of cylindrical micelles in the presence of the dispersed particle additives. This feature can be used as an external switch to control the structure of the particle arrays and thus the optical and electrical properties of composite materials.

2 Materials and methods

The polymer used in this work is supplied by BASF and has a chemical formula corresponding to $PEO_{20}PPO_{70}PEO_{20}$ [6–8]. Pluronic P123 was obtained as a gift from BASF (Mt. Olive, NJ) and was used as received. Lysozyme and bovine-serum albumin (BSA) were purchased as lyophilized powder from Aldrich chemical company (St Louis, MO). Ludox SM-30 (7 nm silica particles) was obtained as a generous gift from Grace Davidson (Columbia, MD) and was used as received. The nominal size of the particles is reported by the manufacturer to

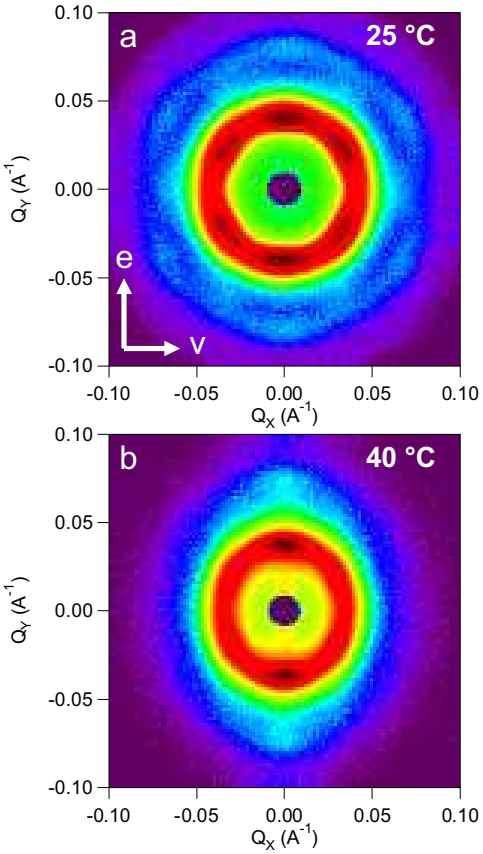

Fig. 2. SANS intensity for a 33 wt% Pluronic P123 sample in pure D_2O at two different temperatures and a shear rate of $10\,s^{-1}$. The neutron beam is perpendicular to the plane defined by the velocity vector (**v**) and the vorticity vector (**e**).

be 7 nm. Heavy water (> 98% D_2O) was purchased from Cambridge Isotopes (Andover, MA).

Neutron scattering experiments are carried out at the NIST Center for Neutron Research (NCNR) in Gaithersburg, MD. The data is collected using the 30 meter SANS instrument NG3. A neutron wavelength of 6 Å with a spread $\Delta\lambda/\lambda$ of 0.15 is used at two detector distances (2, 3.5 m) to gather the scattering profiles. While lower wavelength spreads are possible and might improve the diffraction results, the commensurate loss of flux would be more damaging to the experiments. Improved resolution should really only be achieved by moving to SAXS and, unfortunately, loosing the ability to perform contrast variation.

3 Results and discussion

Figure 2 shows the scattering profiles for a neat polymer sample containing 33 wt% of the tri-block copolymer Pluronic P123 dissolved in pure D_2O. The two-dimensional patterns are such that the velocity axis of the shear plane is parallel to the x-direction and the vorticity is parallel to the y-direction in these images. Even with the poor wavelength resolution of SANS, a significant change in the scattering patterns is observed on a 15 degree increase in temperature. At 25 °C, the samples show Bragg diffraction spots that are consistent with a close-packed crystal (FCC/HCP) of spherical micelles [20–22], while at 40 °C, the patterns are consistent with a crystal of cylindrical micelles at 40 °C [23]. The appearance of diffraction spots in both profiles indicates that the micelle templates are aligned close to a macro-domain crystal where the majority of the micelles have the same lattice and orientation. The position of the diffraction spots in Figure 2a is consistent with an FCC/HCP crystal with a lattice constant of 27 nm and a nearest-neighbor intermicellar distance of 19 nm [21,24]. The position of the first peak is consistent with that seen in the literature [7]. The peaks are not quite that expected of a perfect crystal, but the flow mechanisms of these soft block copolymer materials are complex [20,21,25–27]. Clearly, the solution has attained significant order through the self-assembly and shear orientation. Figure 2b shows bright diffraction spots in the vorticity direction (y-axis) with a spacing that is consistent with the hexagonal packing of cylinders that is expected in these polymer systems ($1 : \sqrt{3} : 2 : \sqrt{7}$) [23]. Although the spacing of the observed peaks is consistent with this lattice, the peak corresponding to $\sqrt{3}$ is missing or it is too weak to be detected. This could be due to the form factor of the micelles, to experimental smearing in SANS, or to the radial orientation of the crystal lattice of cylinders relative to the scattering plane [28]. Assuming hexagonal packing, which is the expected lattice [7,8], the separation between neighboring cylinders at 40 °C corresponds to 19.6 nm. This transition from spherical to cylindrical micelles is also observed macroscopically when the sample is placed between crossed linear polarizers and a light source. The sample at 40 °C (cylinders) is strongly birefringent while at 25 °C (spheres) it is not birefringent. Both the neat and composite samples are birefringent at 40 °C, consistent with the existence of a cylindrical phase.

Figure 3 shows the SANS profiles, at contrast-matched conditions, for a nanocomposite sample that contains bovine-serum albumin (3 wt%) dispersed in a matrix of the tri-block copolymer (33 wt% Pluronic P123) and water. The top profiles (a and b) correspond to the scattering due to the polymer matrix while the bottom profiles (c and d) correspond to the scattering from the dispersed proteins. At 25 °C the scattering shows a diffraction ring in both phases (micelle template and dispersed proteins) with a higher intensity in the direction of the vorticity vector (**e**). Macroscopically, these samples are isotropic between crossed polarizers, so we assume that cubically packed spherical micelles persist on addition of the BSA particulate phase. This assumption is verified by our previous work [3–5]. Unlike Figure 2a, the 25 °C samples with added BSA are not ordered into a single crystal, hence the appearance of a powder ring rather than distinct peaks, which is due to changes in the flow mechanism of these co-crystals [4]. As before, the weakness of the higher order diffraction rings in Figure 3 (a and c) complicate the determination of the lattice structure (FCC/HCP or BCC). Still, the position of the first-order diffraction ring ($q^* = 0.04\,Å^{-1}$) is the same in both phases and corresponds to identical intermicellar (Fig. 3a) and interparticle (Fig. 3c) separation distances of 19.3 nm.

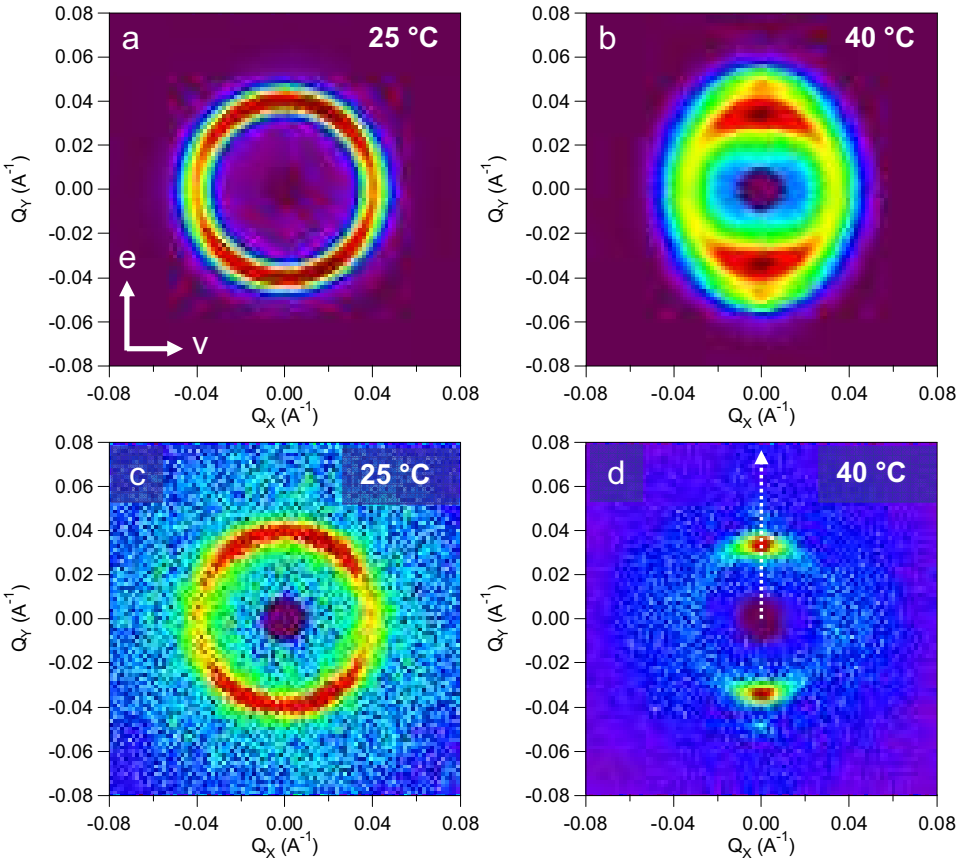

Fig. 3. SANS intensity for a sample that contains 3 wt% serum albumin (BSA) dispersed in a polymer matrix of 33 wt% P123 in aqueous solution at a shear rate of $10\,s^{-1}$. The top profiles (a and b) correspond to the scattering from the micelle template (40% D_2O, 60% H_2O) while the bottom profiles (c and d) correspond to the scattering from the dispersed proteins (13% D_2O, 87% H_2O).

Therefore, the particles are templated in the crystal of spherical micelles even though we are unable to align the crystal into a "single crystal" with the shear field.

When the temperature of the nanocomposite is increased to 40 °C, the diffraction pattern of both phases is characteristic of aligned cylinders in a lattice. The patterns show a similar shift in features as was observed in the neat system (Fig. 2). The appearance of the sharp diffraction spots in both phases demonstrates that the proteins are organized into linear arrays by the template of cylindrical micelles. Macroscopically, the composite system is also birefringent. The proteins, which are located in the interstitial spaces of the crystal, are enclosed laterally by the surrounding micelles and are therefore constrained to lie in a linear "cage". We expect that there are significant defects in these linear arrays (*e.g.*, free spaces and vacancies) because there are no forces that can impart any longitudinal periodicity on the dispersed proteins.

A possible change in the nature of the packing of the cylindrical micelles is demonstrated when the scattering intensity is measured along the vorticity direction (indicated by the dotted arrow in Fig. 3d). The averaged intensity of the cylindrical phases (Figs. 2b, 3b and 3d) along this line are shown in Figure 4. The neat system shows peak positions that are consistent with the more common

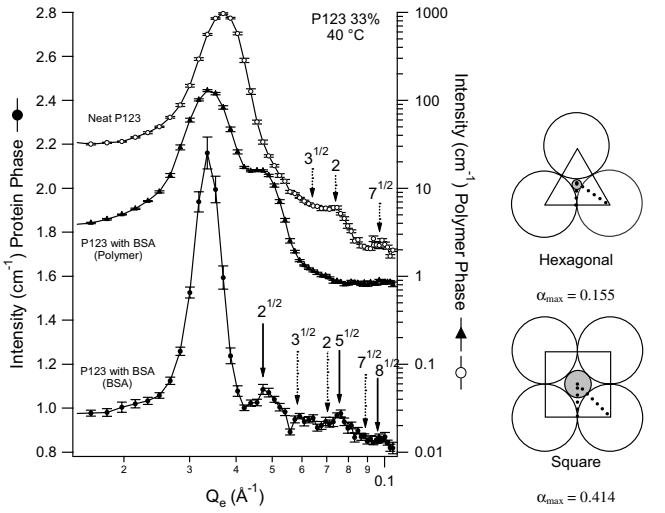

Fig. 4. Linear intensity profiles of Figures 2b, 3b and 3d along the vertical vorticity direction (**e**). The solid arrows indicate the expected position for the diffraction spots for square lattices of cylinders while the dotted arrows indicate the expected position for hexagonal lattices of cylinders. The cross-section of these two lattices and their corresponding interstitial cavities are also sketched.

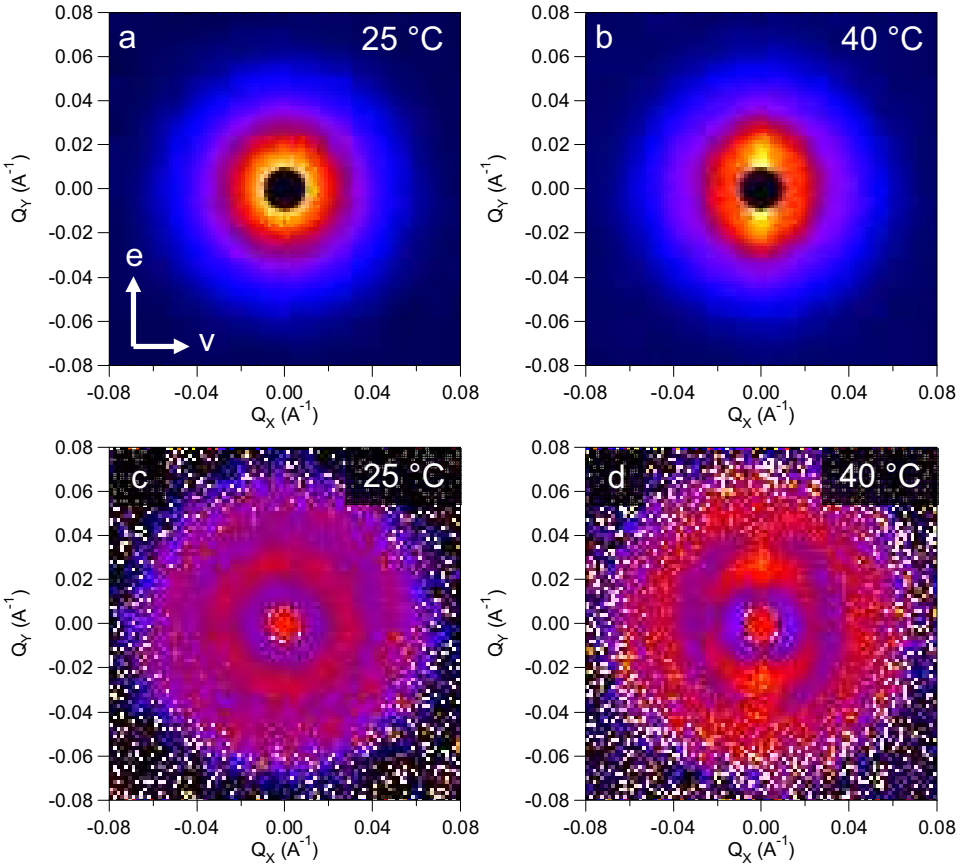

Fig. 5. SANS profiles (a and b) corresponding to the silica particles (polymer is matched) in a nanocomposite containing 4 wt% silica dispersed in a matrix of 33 wt% Pluronic P123 in a solvent of 13% D_2O, 87% H_2O. The bottom profiles (c and d) correspond to the structure factors of the silica particles after the division of the top profiles (a and b) by the form factor of the particles.

hexagonal lattice ($1 : \sqrt{3} : 2 : \sqrt{7}$). However, a change in the relative positions of the peaks is observed in the composite materials. The observed peak spacing in both phases (particles and polymer) of the composite sample is more consistent with cylinders packed in a square lattice ($1 : \sqrt{2} : 2 : \sqrt{5} : \sqrt{8}$). Clearly, the SANS results alone do not provide proof of this change in the cylindrical packing due to the limited resolution and the small number of diffraction peaks. However, the formation of this unusual lattice is justified by considering the relative size of the interstitial cavities in hexagonal and square packing of solid cylinders. The relative size of the interstitial cavity to the diameter of the cylinders is 0.155 in a hexagonal lattice while it is 0.414 for a square lattice. Therefore, the interstitial space in the hexagonal lattice (3 nm) is significantly smaller than the proteins ($D_H \sim 7$ nm) while in the square lattice (8 nm) it is larger. Thus, based on maximum packing, it is more favorable to have a square lattice because the cylinders and the particles will pack more efficiently without requiring significant swelling of the micelle lattice. The separation distance between the micelles and between the linear protein arrays, obtained from the diffraction spots (Fig. 3b and d), is also the same (18.7 nm) for both phases of the nanocomposite and agrees well with the separation of the neat polymer sample (Fig. 2). This shows again that the particles are well templated by the block-copolymer in the cylindrical micelle crystal. The appearance of diffraction spots in the SANS patterns shows that we are able to create a macroscopic sample where the all the linear particle arrays have the same axial orientation.

This simple method can be used to organize a variety of nanometer-sized particles. To demonstrate its versatility, we carried out experiments with silica nanoparticles (Ludox SM) and with lysozyme. The scattering profiles corresponding to the dispersed silica particles (13% D_2O, 87% H_2O) in a similar nanocomposite are shown on the top of Figure 5 (a and b). At 25 °C, we observe an isotropic scattering pattern without any obvious features. At 40 °C we observe that there is a significant anisotropy in the scattering with a larger intensity along the vorticity direction but without clear diffraction spots like those observed in Figures 2 and 3. The cause for these apparently featureless profiles is the decay of the form factor of the silica particles in the q region of interest. To correct for this effect, we divide these scattering profiles by a profile collected at a low temperature (0 °C) when the polymer and particles are disordered and the scattering reflects the shape of the particles (essentially the form factor of the particles). The resulting profiles are shown in Figure 5 (c and d) and correspond to the structure factor of the silica particles. Although the correlation peaks in Figure 5 (c and d) are evident, they are also weaker than those found for the

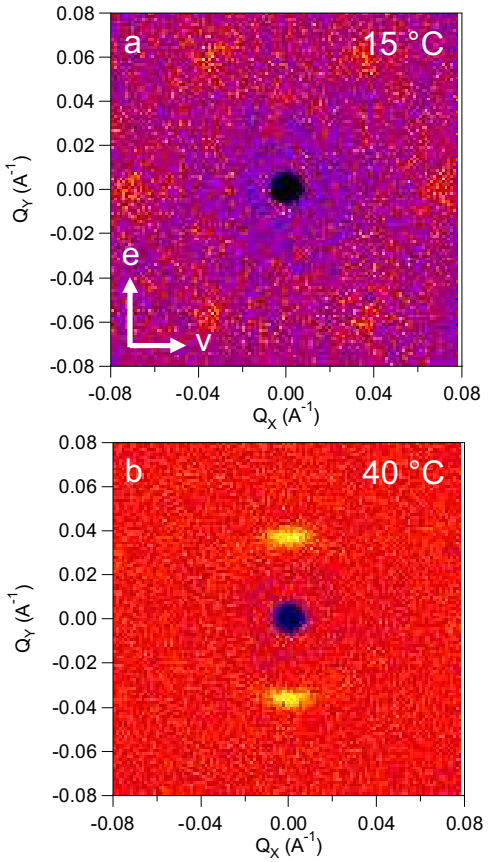

Fig. 6. SANS profiles (a and b) corresponding to the distribution of protein particles in a nanocomposite containing 3 wt% lysozyme ($R_H = 1.95$ nm) [10] dispersed in a matrix of 35 wt% Pluronic P123 in a solvent of 13% D_2O, 87% H_2O.

nanocomposites that contain proteins. This may be due to the larger polydispersity of the silica particles in comparison to the monodisperse proteins. Nevertheless the corrected profiles reveal diffraction spots (Fig. 5d) that are consistent with the silica particles being organized into linear arrays by the cylindrical micelle crystal template. It is also possible that large scale phase segregation occurs due to the addition of particles. Such effect would result in a significant increase in the scattering intensity at low q. Ultra small-angle neutron scattering (USANS) would be necessary to extend the q range in order to identify if phase segregation is occurring as a function of the addition of particles.

Figure 6 shows the scattering profiles for a nanocomposite that contains 3 wt% lysozyme dispersed in a matrix of 35 wt% Pluronic P123 in aqueous solution. In both, the scattering corresponds to the dispersed protein since the solvent has been matched to the SLD of the polymer (13% D_2O, 87% H_2O). At 15 °C (Fig. 6a), the scattering profile has a clear hexagonal pattern of diffraction spots. The position and orientation of the spots indicates that, at this temperature, the lysozyme proteins are organized into a purely FCC lattice with very few stacking faults [21]. Stacking faults, which cause the formation of a mixed FCC/HCP lattice, would result in the appearance of spots at a lower value of q and in the rotation of the orientation of the spots by 30° relative to that observed in Figure 6a [21]. The pattern of an FCC/HCP lattice would be similar to that in Figure 2a. The structure of the nanocomposite at this temperature (Fig. 6a) is analogous to the sodium chloride lattice where the proteins are located in the octahedral interstitial sites between the micelles. The formation of true FCC single crystals was also recently observed in nanocomposites of BSA and Pluronic F127 subjected to oscillatory shear [4]. The interparticle distance, calculated for neighboring proteins in this nanocomposite, corresponds to 17.9 nm. The slightly smaller interparticle spacing is due to the larger polymer concentration that pushes the "soft" polymer micelles closer together [7]. When the temperature is increased to 40 °C, the formation of a linear array of proteins is evident from the two intense diffraction spots in the vorticity direction. The lack of second-order spots is due to the weak form factor of these small proteins. This prevents the determination of the packing lattice (square or hexagonal). Nevertheless, the profile again shows that the proteins are organized into linear arrays by the crystal of cylindrical micelles; a structural transition confirmed by the appearance of optical birefringence in the sample.

4 Conclusions

We have described a simple method to organize a variety of nanosized hydrophilic particles using a self-assembling block copolymer matrix. Temperature is used to drive the polymers to form a crystal of spherical micelles (FCC/HCP) at moderate temperatures to a crystal of cylindrical micelles at higher temperatures. Shear is used to align the micelle template and the dispersed particles towards macroscopic crystal domains with a preferential orientation. Using this technique, the temperature dependence of the polymer template can be used as an external switch to jump between the two types of arrays for the templated nanoparticles. Finally, we show that the technique can be extended to organize a wide variety of particles when the system parameters (*e.g.*, relative size) are chosen appropriately.

This work utilized facilities supported in part by the National Science Foundation under Agreement No. DMR-9986442. We acknowledge the support of the National Institute of Standards and Technology, U.S. Department of Commerce, in providing the neutron research facilities used in this work. DCP acknowledges financial support from the PPG foundation.

References

1. D.C. Pozzo, PhD Thesis (Carnegie Mellon University, Pittsburgh, 2006).
2. D.C. Pozzo, K.R. Hollabaugh, L.M. Walker, J. Rheol. **49**, 759 (2005).
3. D.C. Pozzo, L.M. Walker, Macromol. Symp. **227**, 203 (2005).

4. D.C. Pozzo, L.M. Walker, Macromolecules **40**, 5801 (2007).
5. D.C. Pozzo, L.M. Walker, Colloids Surf. A: Physicochem. Eng. Asp. **294**, 117 (2007).
6. P. Alexandridis, T.A. Hatton, Colloids Surf. A: Physicochem. Eng. Asp. **96**, 1 (1995).
7. G. Wanka, H. Hoffmann, W. Ulbricht, Macromolecules **27**, 4145 (1994).
8. V. Castelletto, I.A. Ansari, I.W. Hamley, Macromolecules **36**, 1694 (2003).
9. K. Mortensen, W. Brown, Macromolecules **26**, 4128 (1993).
10. B. Batas, H.R. Jones, J.B. Chaudhuri, J. Chromatogr. A **766**, 109 (1997).
11. N.L. Almeida, C.L.P. Oliveira, I.L. Torriani, W. Loh, Colloids Surf. B: Biointerfaces **38**, 67 (2004).
12. M. Malmsten, P. Linse, T. Cosgrove, Macromolecules **25**, 2474 (1992).
13. J.A. Baker, J.C. Berg, Langmuir **4**, 1055 (1988).
14. J.S. Higgins, H. Benoît, *Polymers and neutron scattering* (Clarendon Press, Oxford University Press, Oxford, 1994).
15. G.C. Straty, H.J.M. Hanley, C.J. Glinka, J. Stat. Phys. **62**, 1015 (1991).
16. F. Bouchama, M.B. Thathagar, G. Rothenberg, D.H. Turkenburg, E. Eiser, Langmuir **20**, 477 (2004).
17. P.C.A. Alberius, K.L. Frindell, R.C. Hayward, E.J. Kramer, G.D. Stucky, B.F. Chmelka, Chem. Mater. **14**, 3284 (2002).
18. M.R. Bockstaller, E.L. Thomas, Phys. Rev. Lett. **93**, 166106 (2004).
19. S.A. Maier, M.L. Brongersma, P.G. Kik, S. Meltzer, A.A.G. Requicha, H.A. Atwater, Adv. Mater. **13**, 1501 (2001).
20. J. Jiang, C. Burger, C.H. Li, J. Li, M.Y. Lin, R.H. Colby, M.H. Rafailovich, J.C. Sokolov, Macromolecules **40**, 4016 (2007).
21. W. Loose, B.J. Ackerson, J. Chem. Phys. **101**, 7211 (1994).
22. G. Schmidt, W. Richtering, P. Lindner, P. Alexandridis, Macromolecules **31**, 2293 (1998).
23. S. Forster, A. Timmann, M. Konrad, C. Schellbach, A. Meyer, S.S. Funari, P. Mulvaney, R. Knott, J. Phys. Chem. B **109**, 1347 (2005).
24. G.A. Mcconnell, M.Y. Lin, A.P. Gast, Macromolecules **28**, 6754 (1995).
25. V. Castelletto, I.W. Hamley, P. Holmqvist, C. Rekatas, C. Booth, J.G. Grossmann, Colloid Polym. Sci. **279**, 621 (2001).
26. C. Daniel, I.W. Hamley, W. Mingvanish, C. Booth, Macromolecules **33**, 2163 (2000).
27. E. Eiser, F. Molino, G. Forte, X. Pithon, Rheol. Acta **39**, 201 (2000).
28. A. Guinier, *X-ray Diffraction in Crystals, Imperfect Crystals, and Amorphous Bodies* (Dover Publications, New York, 1963).